NASA TECHNICAL MEMORANDUM

NASA TM X-1435

NASA TM X-1435

EVALUATION OF SCREECH SUPPRESSION CONCEPTS IN A 20 000-POUND THRUST-HYDROGEN-OXYGEN ROCKET

by John P. Wanhainen, Ned P. Hannum, and Louis M. Russell

Lewis Research Center

Cleveland, Ohio

NATIONAL AERONAUTICS AND SPACE ADMINISTRATION • WASHINGTON, D. C. • AUGUST 1967

NASA TM X-1435

EVALUATION OF SCREECH SUPPRESSION CONCEPTS IN A 20 000-POUND THRUST-HYDROGEN-OXYGEN ROCKET

By John P. Wanhainen, Ned P. Hannum, and Louis M. Russell

Lewis Research Center
Cleveland, Ohio

NATIONAL AERONAUTICS AND SPACE ADMINISTRATION

For sale by the Clearinghouse for Federal Scientific and Technical Information
Springfield, Virginia 22151 – CFSTI price $3.00

EVALUATION OF SCREECH SUPPRESSION CONCEPTS IN A 20 000-POUND THRUST-HYDROGEN-OXYGEN ROCKET

by John P. Wanhainen, Ned P. Hannum, and Louis M. Russell

Lewis Research Center

SUMMARY

An experimental investigation was conducted at the Lewis Research Center to determine the effects of (1) propellant injection radial distribution, (2) fluorine additive to the liquid oxygen, (3) extended oxidizer tubes, (4) porous injector faceplate, (5) nozzle area radial distribution, and (6) chamber wall film cooling on acoustical mode stability characteristics. Stability data were obtained at a chamber pressure of 300 pounds per square inch absolute and over a range of oxidant-fuel ratios from 3.5 to 6.5. Hydrogen injection temperature was used to rate the stability of the various designs. The combustor with the lowest self-triggering temperature was considered to be the most stable design.

Concentrating the propellant injection radial distribution had a detrimental effect on longitudinal mode stability. Addition of fluorine to the oxygen to an amount of 30 percent by weight had no significant effect on stability; however, characteristic exhaust velocity efficiency was improved by 1 to 3 percentage points. The combustor stability characteristics were significantly improved by the wagon wheel nozzle, the porous faceplate, and the extended oxidizer tubes. Chamber wall film cooling produced no major change in the hydrogen temperature stable operating limits. Performance, however, decreased 2 to 3 percentage points for each 10 percent of hydrogen flow diverted for film cooling.

INTRODUCTION

The NASA Lewis Research Center is presently conducting an extensive experimental program exploring combustion dynamics of hydrogen-oxygen propellant rockets. The objectives of the program are twofold; first, achieving an adequate understanding of screech to provide a firm theoretical base from which future designs can be made, and second, providing semiempirical design rules applicable to hydrogen-oxygen engine systems. Experiments in the program have included studies of acoustic damping upon insta-

bility (refs. 1 and 2) as well as controlled testing of motors with parametric variations intended to determine the parameters that have the strongest influence on stability (ref. 3 and other NASA unpublished data), As a part of this overall effort, an investigation of the effects of the following on screech were investigated: (1) propellant injection radial distribution, (2) fluorine additive to oxygen, (3) extended oxidizer tubes, (4) porous injector faceplates, (5) nozzle radial area distribution, and (6) chamber wall film cooling. The rationale behind each will be covered in the RESULTS AND DISCUSSION.

The experiments were conducted with concentric-tube-type injectors in 20 000-pound (89 000-kN) thrust engines operating at a nominal chamber pressure of 300 pounds per square inch (2070 kN/sq m). The contraction ratio of the combustor, with the exception of those used for propellant injection distribution experiments, was 1.9. The engine size was chosen to allow reasonable flexibility and to minimize cost and yet be large enough to allow confidence in the applicability of test results to large engines.

Hydrogen injection temperature was used to rate the stability characteristics of the various screech suppression concepts. The rating criterion and the hydrogen temperature ramping technique utilized in this investigation were obtained from reference 3, where it was shown that the effects of hydrogen temperature on screech are related to the change in hydrogen density and the corresponding change in hydrogen-to-oxygen injection velocity ratio (or related parameter).

APPARATUS

Test Facility

The Rocket Engine Test Facility of the Lewis Research Center is a 50 000-pound (222 500 kN) thrust sea level stand equipped with an exhaust gas muffler and scrubber. A sketch of the facility is shown in figure 1. The facility utilized a pressurized propellant system to deliver the propellants to the engine from the storage tanks. The oxygen propellant line was immersed in a nitrogen bath, and the liquid hydrogen line was insulated with a plastic foam. The propellant storage tanks consisted of a 175-cubic-foot (4. 95-CU-m) liquid hydrogen Dewars, a 120 000-standard-cubic-foot (3400-cu-m) gaseous hydrogen bottle farm, and a 55-cubic-foot (1.56-cu-m) liquid oxygen tank submerged in a liquid nitrogen bath.

The engine was mounted on the thrust stand (fig. 2) to fire vertically downward into the scrubber where the exhaust gases were sprayed with water at rates to 50 000 gallons per minute (189 cu m/min) for the purpose of cooling and sound suppression. The cooled exhaust gases were discharged into the atmosphere from the 70-foot-high (21-m) exhaust stack.

The facility was operated remotely from a control room located 2000 feet (610 m) from the facility. In addition to the central data recording system, the facility was equipped with several direct reading oscillographs and a tape recorder to record test results.

Engine

The basic engine (fig. 3) was comprised of an injector, a cylindrical heat-sink thrust chamber with a 10.78-inch (0.274-m) inside diameter, and a convergent-divergent exhaust nozzle with a contraction ratio of 1.9 and an expansion area ratio of 1.3. The expansion ratio was picked for the convenience of operation of the test since it had no effect on the combustion process. Schematics of the standard engine, along with other variations in thrust chamber and nozzle geometry used in this investigation, are shown in figure 4. The inner surfaces of the mild steel heat-sink combustion chambers and nozzle were coated with 0.030-inch-thick (0.000'762-m) flame-sprayed zirconium oxide to reduce the rate of heat transfer into the metal. This allowed a test duration of 3 seconds which was adequate to obtain test results.

Injector

Concentric-tube-type injectors, each element consisting of a central oxidizer tube surrounded by a concentric hydrogen annulus, were used in the investigation. The concentrated pattern injector (fig. 5(a)) consisted of a bundle of 100 oxidizer tubes spaced apart so that the void area between the tubes equaled the hydrogen flow area of a conventional 100-element concentric tube injector. The pattern diameter was 4.01 inches. A cross-sectional view of the injector is shown in figure 5(b). Faceplate and cross-sectional views of the 421-element injector which was used to evaluate the effects of fluorine additive, porous faceplate, nozzle radial position, and film cooling are shown in figure 5(c). The faceplate of the injector was removable and was fabricated from 1/2-inch-thick (0.00127-m), oxygen-free copper. Figure 5(d) shows the same injector with a porous stainless steel faceplate. The porosity of the material was defined by the manufacturer in terms of flow rate which was 120 standard cubic feet per minute (3.4 cu m/min) of air at 70° F (295° K) at a differential pressure of 2 pounds per square inch (13.8 kN/sq m). The oxidizer tube extension program was conducted using a 100-element injector shown in figure 5(e). In the photograph, the oxidizer tubes which were fabricated from Hastalloy were extended $1\frac{1}{4}$ inches (0.032 m).

Hydrogen Temperature Controller

The hydrogen temperature ramp was accomplished by starting the run on a mixture of liquid hydrogen and warm gaseous hydrogen and then reducing the percentage of gas introduced in a predetermined ramp while simultaneously opening the liquid hydrogen valve to maintain a constant total flow. Mixing was accomplished by swirling the liquid into the gaseous hydrogen stream (fig. 6). The mixing station was in a manifold outside the injector with an intervening volume of 1140 cubic inches (0.0187 cu m). Flow rates of gaseous hydrogen and liquid hydrogen to the mixer were controlled with valves that were operated by an electrohydraulic servosystem.

Instrumentation

Locations for the various transducers are shown on a schematic diagram of the engine and associated plumbing in figure 7. The signals from the transducers were transmitted to the control room and to the Center's automatic digital data recording system. Piezoelectric-type, water-cooled, flush-mounted pressure transducers were used at three locations on the thrust chamber (fig. 7) to determine the character and phase relationship of the pressure field and allow identification of the screech mode. The response characteristics of the transducers as installed are flat to within 10 percent to a frequency of 6000 hertz and have a nominal resonant frequency of about 20 000 hertz in the water-cooled mount. The signals from high frequency response transducers were recorded in analog form on magnetic tape and, in addition, were displayed on direct reading instruments for visual monitoring during the tests.

Oxygen propellant flow rate was determined with a turbine-type flowmeter which was calibrated with water using a static weighing system. The correction from water calibration to cryogenic calibration that accounted for the dimensional change of the instrument with temperature was obtained from the flowmeter manufacturer. Liquid hydrogen flow rate was measured using a venturi submerged in the liquid hydrogen tank, and the gaseous hydrogen flow rate was measured using an orifice plate. The strain-gage-type pressure transducers were calibrated against a commercial standard. The liquid flow temperatures were measured by platinum resistance-type sensors described in reference 4. The hydrogen injection temperature was measured using four carbon resistance-type probes (ref. 5) that were installed as illustrated in figure 3. The pressure and temperature systems were calibrated immediately prior to data acquisition by an electrical two-step calibration system, which used resistances in an electrical circuit to simulate given conditions.

PROCEDURE

As mentioned in the INTRODUCTION, the stability rating of each configuration was expressed in terms of the hydrogen temperature at which screech was encountered. The technique employed was to select an initial hydrogen temperature by presetting the valves of the mixer and, about 1/2 second after ignition, ramping the gas valve toward a closed position and the liquid valve toward an open position to reduce the temperatureof the injected hydrogen to a value below the anticipated screech limit. After the first transition point was obtained for a configuration, the ramp rate was reduced to minimize mass accumulation in the propellant system. The screech limit was obtained from high-speed recorder data wherein the hydrogen temperature in the injector cavity was read at the instant screech was indicated by an oscillograph trace of a flush-mounted pressure transducer. Combustion was considered unstable when a periodic wave-form with an amplitude substantially greater than the normal noise level (10 to 15 psi (68.9 to 103.5 kN/sq m) peak to peak) was observed on the oscillograph record. A typical screech transition is presented in the RESULTS AND DISCUSSION section. Data were obtained over a range of oxidant-fuel ratios to establish a limit curve.

For those configurations that exhibited low screech temperatures, below about 70° R (38.9° K), it was necessary to prechill all hydrogen lines and valves down to the fire valve by a preflow and overboard venting of liquid nitrogen. In addition, still lower temperatures in the 55° to 65° R (30.5° to 36.1° K) temperature range required the use of a 1-second lead of liquid hydrogen through the injector for prechill prior to stepping the mixer to the preset condition. Because of the use of heat-sink thrust chambers and nozzles, it was necessary to limit run duration to 3 seconds; accordingly, all valve scheduling was accomplished by the use of an automatic sequence timer. Ignition of the engine was accomplished by injecting a small amount of fluorine into the oxidizer line immediately upstream of the injector simultaneously with actuation of the oxidizer fire valve.

RESULTS AND DISCUSSION

In this investigation, hydrogen injection temperature was used to rate the screech stability characteristics of the various combustor designs. The combustor with the lowest self-triggering temperature was considered to be the most stable design. A typical temperature ramp test to determine the stable operating limits of a given design is shown in figure 8. The hydrogen temperature at the start of the test illustrated was about 180° R (100° K) and was then ramped down through the transition point which was about 140° R (78° K). Stability plots in terms of this transition temperature (minimum

stable hydrogen temperature) are presented as a function of the oxidant-fuel ratio for each design. Typical amplitude spectral density graphs are also presented for each injector at a hydrogen temperature operating condition of about 60° R (40° K).

Effect of Propellant Injection Distribution on Stability

The velocity difference between combustion gas and liquid droplets has been shown to be an important parameter in controlling the transverse mode stability characteristics in the theoretical model of reference 6. Figure 9 (from ref. 6) shows this dependence. It can be seen that as the differential velocity was increased, larger disturbances were required to initiate instability. Since combustion gas velocity is related to the chamber geometry, increasing the velocity differential parameter to effect stable combustion (transverse mode) can be accomplished by simply altering the shape of the thrust chamber. Unfortunately, as will be shown in a later part of this section, the alterations made to the injector (fig. 5) and to the chamber to obtain high velocity differentials resulted in a change of the predominant mode instability from first tangential to first longitudinal. Thus, the comparison of the effects obtained in this experiment with the model of reference 6 are, therefore, invalid.

Typical stability results for chambers employing a divergence section to increase the combustion gas velocity axial profile (thereby increasing the combustion gas-liquid droplet velocity differential) are shown in figure 10. Examination of the results shows that concentrating the combustion had a detrimental effect on the hydrogen temperature stable operating limits. Whereas a conventional 100-element injector (10.78-in.-diam. (0.274 m) uniform pattern) was marginally stable at a hydrogen injection temperature of 60° R (33.3° K) (dashed line), the transition temperature of the 60° tapered chamber (fig. 4(a)) was 125° R (69.4° K) at an oxidant-fuel ratio of 5. The temperature limit boundary for the 30° tapered chamber (fig. 4(b)) could not be established because of facility limitations; however, it was unstable at temperatures higher than 240° R (133.3' K).

The mode of instability that was encountered was longitudinal (determined from phase relationships); however, the frequency of the oscillation did not correspond to the calculated frequency for the chamber and environment. The calculated frequency corresponding to the first longitudinal mode for the chamber is about 1900 hertz. As seen in figure 11, maximum pressure amplitudes occurred at frequencies of 3100 and 2350 hertz for the 30° and 60° tapered chambers. Cold flow tests of reference 7 indicate that tapering of the chamber changed the wave reflection and gas particle motion so that the chamber is acoustically shortened to the longitudinal mode, but not to the extent observed in the results of figure 11. It must be noted that extremely high injector face pressures

were recorded during tests of the tapered chamber (table I) indicating that possibly thermal choking occurred. Should this have been the case, the instability observed may not have been the usual acoustic mode but rather one related to an unstable shock system. In any event, since a transverse mode of instability was not encountered in the tests, no conclusion can be made from the results as to the validity of the analytical transverse mode stability considered in reference 6.

As a matter of interest, the effect of varying the nozzle throat diameter or contraction ratio on the longitudinal mode stability characteristics of the concentrated pattern injector in cylindrical combustor is shown in figure 12. The hydrogen temperature stable operating limits were improved by decreasing the nozzle throat diameter. In combustors with contraction ratios of 1.9, 3, and 4.5 (fig. 4), the screech transition temperatures were 95° (52.8° K), 74° (41.1° K), and 68° R (37.8° K), respectively. It must be noted, however, that the total propellant weight flow was decreased in proportion to the change in nozzle throat area to maintain a nominal 300-pound-per-square-inch-absolute (2070 kN/sq m) chamber pressure; thus, the improved stability limits with decreasing nozzle size may not entirely be the effect of contraction rato. The mode of instability was first longitudinal as can be seen in figure 13. Concentrating propellant into the tenter of the chamber should improve tangential mode stability, as was found in the experiment, and promote the radial mode of instability (ref. 8). Since only a longitudinal mode occurred, it was concluded that concentrating the combustion into the center of the chamber apparently altered the axial distribution of the combustion process to favor this mode.

The improvement in longitudinal mode stability characteristics as the nozzle contraction ratio was increased is in general agreement with predicted trends by the theoretical analysis of reference 9. The analysis indicates that the longer the region (subsonic portion of the nozzle) over which the velocity gradient is spread, the more the reflection pattern will be dispersed and, thus, the smaller the chance of resonance and instability.

Characteristic exhaust velocity efficiency of the 100-element concentrated pattern injector during stable operation just prior to screech is presented in figure 14 as a function of oxidant-fuel ratio. Data are presented for tests conducted only in cylindrical chambers because the momentum pressure loss correction for tapered chambers was not considered sufficiently accurate to present. At an oxidant-fuel ratio of 5, the injector had a characteristic exhaust velocity efficiency of about 96 percent.

Effect of Fluorine Additive to Liquid Oxygen

The stable combustion operating experience at the Center with hydrogen-fluorine propellant systems suggested the investigation of the use of fluorine additive to the liquid oxygen as a possible cure for combustion instability. The concentration of fluorine in the

oxygen evaluated was approximately 30 percent by weight. A standard engine configuration consisting of a 421-element, concentric-tube injector (fig. 5(c)), a 10.78-inch-diameter (0.274 m) cylindrical thrust chamber, and a nozzle with a contraction ratio of 1.9 was used for the tests.

The screech characteristics (minimum stable hydrogen temperature) of the combustor using hydrogen - fluorine-oxygen mixtures and hydrogen-oxygen are compared in figure 15. The hydrogen temperature at transition is presented as a function of equivalence ratio (ratio of oxidant-fuel ratio to stoichiometric oxidant-fuel ratio). If it is assumed that both propellant systems will be operated at the same equivalence ratio, addition of fluorine into the oxygen in amounts to 30 percent by weight produce no significant change in hydrogen temperature stable operating limits. Addition of fluorine to the oxygen, however, did have a significant effect on engine performance (fig. 15(b)). When operating with fluorine-oxygen mixtures, the combustor produced a characteristic exhaust velocity of about 99 percent of theoretical shifting (fluorine-oxygen mixtures) which was an improvement of 1 to 3 percentage points (depending on the equivalence ratio) compared to the performance with 100 percent oxygen.

Examination of the amplitude spectral density graphs presented in figure 16 shows that the mode of instability (encountered as the hydrogen temperature was reduced) did not change with the addition of fluorine. In both cases, the predominant pressure spike (150 psi (1055 kN/sq m)) occurred at frequencies between 3000 and 3500 hertz which corresponds to the first tangential mode for the combustor.

Effect of Porous Injector Faceplate

The mechanism proposed in reference 8 for the growth of pressure oscillations in a rocket motor is one where a small random pressure disturbance increases the burning rate through compression effects and, in turn, is amplified because hot combustion gases are being produced at a rate faster than at steady-state combustion pressure. Reflected oscillations from the solid injector face or chamber walls are further amplified as they again pass through the unburned mixture. It was hypothesized that porous injector faceplates, which are used in many current hydrogen-oxygen engines, should absorb energy and thereby reduce the strength of the reflected waves. This type of faceplate should, therefore, be a combustion stabilizing device. For the aforementioned model, porous faceplates should be more effective in stabilizing longitudinal than transverse oscillations in the chamber.

The screech stability characteristics of a 421-element concentric tube injector incorporating nonporous (fig. 5(c)) and porous faceplates (fig. 5(d)) are compared in figure 17(a). Even though the predominant mode of instability for the basic injector was

tangential, a significant improvement of about 25° R (13.9° K) in hydrogen temperature stable operating limits was observed with the injector incorporating the porous face. It must be noted, however, that the tests were conducted with an injector with poor stability characteristics and the marked effect of faceplate porosity on stability would not likely be the same in terms of hydrogen temperature for more stable injector designs. Also shown in figure 17 is the effect of a porous injector faceplate on engine performance. The weight flow of hydrogen through the porous material was calculated to be approximately 5 percent of the total hydrogen weight flow to the engine. Examination of figure 17(b) shows that the effect of diverting about 5 percent of the hydrogen for faceplate cooling was to reduce characteristic exhaust velocity efficiency by about $1\frac{1}{2}$ percentage points.

A typical amplitude spectral density graph of screeching combustion with the porous faceplate injector is shown in figure 18. The modes of instability of first tangential (predominant) and second longitudinal (3900 Hz) encountered with the porous faceplate injector were the same as the solid face design (fig. 16(a)).

Effect of Oxygen Tube Extension

Since combustion instability in hydrogen-oxygen systems generally occurs only at reduced hydrogen injection temperature (low hydrogen to oxygen injection velocity ratios), it appeared that the problem could be avoided if some method could be employed to increase hydrogen temperature. In large high pressure regenerative engines, the designer usually has little, if any, chamber cooling margin, thus, there is little latitude for hydrogen temperature to the injector (cooling jacket outlet) to be increased. The design philosophy of the extended tube injector was to delay mixing of the propellants until the temperature of the hydrogen was increased to a stable operating temperature by heat transfer from the hot recirculated combustion gases.

The screech stability characteristics of a 100-element concentric tube injector incorporating extended ($1\frac{1}{4}$-in. (0.032 m)) oxidizer elements and flush oxidizer elements are compared in figure 19(a). Whereas screech was encountered at a hydrogen injection temperature of about 78° R (43.3° K) (oxidant-fuel ratio of 5) with the flush elements, the $1\frac{1}{4}$-inch extended tubes provided stable combustion to the minimum temperature of 60° R (33.3° K) attainable in the facility. It must be noted, however, that the improvement in stability was accompanied by a reduction in engine performance (fig. 19(b)); thus the change in stability may, in fact, have resulted from the performance decay rather than an increase of the hydrogen temperature prior to combustion. At a hydrogen injection temperature of 60° R (33.3° K), the characteristic exhaust velocity efficiency was about 80 percent at an oxidant-fuel ratio to 5. Also included on the figure are performance data with the extended tube injector at a hydrogen injection temperature of 80° R (44.5° K).

Even at this temperature level (which corresponds to transition temperature of flush element configuration of an oxidant-fuel ratio of 5), the characteristic exhaust velocity efficiency was about 4 percentage points lower than the flush element injector.

Typical chamber pressure oscillations during operation at a hydrogen temperature of 60° R for both the flush and extended oxidizer tube injector configurations are shown in figure 20. As can be seen in figures 20(a) and 20(b), the mode of instability encountered with the flush tube configuration was not always the same and varied from first tangential (3200 Hz) to second tangential (5300 Hz) between tests. Examination of figure 20(c) shows that the injector with $1\frac{1}{4}$-inch (0.274 m) tube extension was free of any high frequency oscillations. The low frequency oscillation still present is a feed system associated or chugging type of instability.

The postfire condition of the extended oxidizer tube injector, after five firings with a total duration of about 10 seconds, is shown in figure 5(e). Only seven oxidizer tubes (located in the inner rows) suffered any damage by tip erosion. The two outermost rings of oxidizer tubes were undamaged.

Effect of Nozzle Area Radial Distribution

This part of the investigation was a cursory examination of the possibility of improving tangential mode stability characteristics (minimum stable hydrogen temperature) of the combustor by increasing acoustic flow losses through the exhaust nozzle. It was hypothesized that, at the hydrogen temperature screech boundary, a state exists where the acoustic energy gains equal the acoustic energy losses of the combustor. An increase, therefore, in acoustic energy losses should result in lowering the minimum stable hydrogen temperature. Results of reference 10 indicate that that flow dependent losses through a vent (nozzle) increase as the vent is moved toward the pressure antinode. In this case of a tangential mode of instability, the region of high energy potential (pressure antinode) is at the walls of the combustor; thus, for maximum losses, the nozzle open area should be positioned at the periphery of the combustor. Accordingly, a nozzle was fabricated with an internal plug and eight radial support spokes (wagon wheel) as shown in figure 21. The nozzle was evaluated with the 421-element concentric tube injector (fig. 5(c)) and a cylindrical combustion chamber.

The stability characteristics of a combustor with a conventional convergent-divergent nozzle and the annular flow (wagon wheel) nozzle are compared in figure 22. The hydrogen temperature stable operating limits were improved about 20° R (11.1° K) with the wagon wheel nozzle compared to the conventional configuration. The limited success of the wagon wheel configuration may be due to its distant location from the region of highest energy release (maximum screech amplitude) which normally occurs near the injector

(ref. 11). Possibly, at the plane of the nozzle, the wave had decayed in amplitude such that only a small increase in flow losses was obtained with the wagon wheel nozzle configuration.

The longitudinal mode stability characteristics were expected to deteriorate with the wagon wheel nozzle which had short subsonic length (ref. 12). However, as can be seen by comparing the results of figure 23(a) and figure 16(a), the nozzle appeared to have a stabilizing effect on this mode. The amplitude of the first tangential mode (3500 Hz) was about the same as with the conventional nozzle (fig, 16(a)). In certain tests of this configuration, beating between the first tangential and second longitudinal modes was observed. The high frequency pressure transducer output trace is shown along with the amplitude spectral density graph for such a test in figure 23(b). As can be seen, the oscillograph trace had a modulating sinusoidal characteristic of beating, similar to the results of cold acoustic tests reported in reference 2.

Effect of Chamber Wall Film Cooling

Heat-transfer analyses have indicated that hydrogen-oxygen regeneratively cooled engines may have to employ some supplemental cooling to prevent excessive hot-side tube wall temperatures at high chamber pressure operating conditions. One cooling technique, that has been used in many engines and is particularly effective in hydrogen fuel systems because of its high heat capacity, is film cooling. This method of cooling, however, changes the propellant mass flux radial distribution which has been shown in reference 8 to have a significant effect on acoustical mode stability characteristics. For example, concentrating propellants at the walls of the combustor was found to promote a tangential mode of instability. The object of this phase of the investigation was, therefore, to determine the effect, if any, of chamber wall film cooling and the resulting change in mass flox distribution on the transverse mode stability characteristics. A 421-element injector was used in the investigation.

The stability and performance characteristics of the injector utilizing 10 and 20 percent of the total hydrogen weight flow for film cooling are compared to the basic injector (without film cooling) in figure 24. The scatter in the stability data (fig. 24(a)) makes it difficult to ascertain any effect of chamber wall film cooling on hydrogen temperature stable operating limits. Possibly, the stability characteristics of the combustor deteriorated slightly at high oxidant-fuel ratios of 6 with the provision of film cooling. A definite reduction in performance (fig. 24(b)), however, was observed as the percent film cooling was increased. Characteristic exhaust velocity efficiency decreased 2 to 3 percentage points for each 10 percent of film cooling.

SUMMARY OF RESULTS

An experimental investigation was conducted at the Lewis Research Center to determine the effects of propellant injection radial distribution, fluorine additive to the liquid oxygen, extended oxidizer tubes, porous injector faceplate, nozzle area radial distribution, and chamber wall film cooling on acoustical mode stability characteristics. The investigation yielded the following results:

1. Concentrating the injection distribution into the center of the combustor had a detrimental effect on longitudinal mode stability. Increasing the engine contraction ratio by decreasing the nozzle throat diameter lowered the hydrogen temperature at which screech (first longitudinal mode) was encountered.

2. Addition of fluorine to the oxygen to an amount of 30 percent by weight produced no significant effect on the stability characteristics of a 421-element injector. Engine performance, however, increase 1 to 3 percentage points with fluorine-oxygen mixtures.

3. Provision of porous injector faceplates improved the hydrogen temperature operating limits of a 421-element injector by 25° R (13.9° K) over the range of oxidant-fuel ratios investigated.

4. Extending the oxidizer tubes $1\frac{1}{4}$ inches (0.274 m) from the injector face stabilized the combustion of a 100-element injector to minimum temperature attainable in the facility (60° R (33.3° K)); however, the improvement in stability was accompanied by a loss in performance.

5. The wagon wheel nozzle improved the hydrogen temperature transverse mode operating limits by 20° R (11.1° K).

6. Provision of chamber wall film cooling up to 20 percent of the total fuel flow produced no major change in the stability characteristics of the combustor. Performance decreased 2 to 3 percentage points for each 10 percent of the total hydrogen weight flow diverted for film cooling.

Lewis Research Center,
National Aeronautics and Space Administration,
Cleveland, Ohio, April 10, 1967,
128-31-06-05-22.

REFERENCES

1. Wanhainen, John P.; Bloomer, Harry E.; Vincent, David W.; and Curley, Jerome K.: Experimental Investigation of Acoustic Liners to Suppress Screech in Hydrogen-Oxygen Rockets. NASA TN D-3822, 1967.

2. Phillips, Bert; and Morgan, C. Joe: Mechanical Absorption of Acoustic Oscillations in Simulated Rocket Combustion Chambers. NASA TN D-3792, 1967.

3. Wanhainen, John P.; Parish, Harold C.; and Conrad, E. William: Effect of Propellant Injection Velocity on Screech in 20,000-Pound Hydrogen-Oxygen Rocket Engine. NASA TN D-3373, 1966.

4. Ladd, J. W.: A Durable and Reliable Test Stand System for High Accuracy Temperature Measurements in the Cryogenic Ranges of Liquid Hydrogen and Liquid Oxygen. Advances in Cryogenic Engineering. Vol. 6, K. D. Timmerhaus, ed., Plenum Press, 1961, pp. 388-395.

5. Herr, Austin C.; Terbeek, Howard G.; and Tieferman, Marvin W.: Suitability of Carbon Resistors for Field Measurements of Temperatures in the Range 35° to 100° R. NASA TN D-264, 1960.

6. Priem, Richard J.; and Guentert, Donald C.: Combustion Instability Limits Determined By a Nonlinear Theory and a One-Dimensional Model. NASA TN D-1409, 1962.

7. Wieber, Paul R.: Acoustic Decay Coefficients of Simulated Rocket Combustors. NASA TN D-3425, 1966.

8. Zucrow, M. J.; Osborn, J. R.; and Bonnell, J. M.: High Frequency Combustion Pressure Oscillations in Motors Burning Gaseous Propellants. Rep. No. TM-65-5, JPC-409, Purdue University, Jet Prop. Center, Aug. 1965.

9. Crocco, Luigi; and Cheng, Sin-I: Theory of Combustion Instability in Liquid Propellant Rocket Motors. Butterworth Scientific Publ., 1956.

10. Gordon, Colin; and Smith, P. W., Jr.: Acoustic Losses of a Resonator with Steady Gas Flow. Acoust. Soc. Am. J., vol. 37, no. 2, Feb. 1965, pp. 257-267.

11. Clayton, R. M.; and Rogero, R. S.: Experimental Measurements on a Rotating Detonation-Like Wave Observed During Liquid Rocket Resonant Combustion. Tech. Rep. 32-788 (NASA CR-67259), Jet Propulsion Lab., California Inst. Tech., Aug. 15, 1965.

12. Nord, W. J., ed.: Gemini Stability Improvement Program. Vol. 3: Analytical Model. (AFSSD-TR-66-2, AD-626766), Rep. No. GEMSIP-FR-1, Aerojet-General Corp., Aug. 31, 1965.

TABLE I. - EXPERIMENTAL DATA

Test	Hydrogen injection temperature		Static pressure of injector		Hydrogen weight flow, W_{H_2}		Oxygen weight flow, W_{H_2}		Oxidant-fuel ratio, O/F	Oxygen injector pressure drop		Hydrogen injector pressure drop		Efficiency of characteristic exhaust velocity, η_C^*, percent	Number of injector elements	Chamber taper, deg	Film cooling, percent	Tube extension		Nozzle contraction ratio, A	Equivalence ratio	Stability classification
																		in.	cm			
	°R	°K	psi	N/sq m	lb/sec	kg/sec	lb/sec	kg/sec		psi	N/sq m	psi	N/sq m									
Injection distribution studies																						
722	99	55.0	---	---------	11.3	4.99	56.1	25.45	4.95	131	0.903 $\times 10^6$	58	0.399 $\times 10^6$	-----	100	0	--	--	------	1.9	-----	Transition
723	97	53.9	---	---------	10.9	4.94	54.8	24.86	5.01	103	.710	38	.262	-----		0	--	--	------		-----	
724	85	47.2	---	---------	12.1	5.49	50.4	22.86	4.15	84	.579	35	.241	-----		0	--	--	------		-----	
719	106	58.9	---	---------	10.9	4.94	45.5	20.64	4.14	80	.552	51	.352	-----		60	--	--	------		-----	
720	125	69.4	398	2.744×10^6	10.4	4.71	52.1	23.63	5.03	98	.676	47	.324	-----		60	--	--	------		-----	
721	131	72.8	418	2.882	10.3	4.67	53.5	24.27	5.20	102	.703	48	.331	-----		60	--	--	------		-----	
773	238	132.2	663	4.571	10.9	4.94	46.9	21.27	4.31	64	.441	77	.531	-----		30	--	--	------		-----	Unstable
774	249	138.3	678	4.675	10.2	4.63	52.6	23.86	5.18	83	.572	79	.545	-----		30	--	--	------		-----	Unstable
94	79	43.9	289	1.993	6.7	3.04	28.5	12.93	4.25	---	----------	21	.145	102.2		0	--	--	------	3.0	-----	Transition
95	76	42.2	325	2.241	6.7	3.04	36.5	16.56	5.39	---	----------	18	.129	96.7			--	--	------		-----	
96	70	38.9	316	2.179	7.4	3.36	34.2	15.51	4.59	---	----------	20	.138	95.4			--	--	------		-----	
97	72	40.0	316	2.179	7.7	3.49	32.5	14.74	4.22	---	----------	22	.152	98.0			--	--	------		-----	
82	67	37.2	295	2.034	4.4	1.99	20.6	9.34	4.70	34	.234	9	.062	97.7			--	--	------	4.5	-----	
83	68	37.8	313	2.158	4.0	1.81	23.7	10.75	5.92	22	.152	11	.0758	96.9			--	--	------		-----	
84	66	36.7	301	2.075	4.3	1.95	22.2	9.98	5.20	14	.0965	17	.117	95.4			--	--	------		-----	
85	71	39.4	315	2.172	5.0	2.27	20.6	9.34	4.10	55	.379	46	.317	100.4			--	--	------		-----	
86	65	36.1	290	1.999	4.3	1.95	21.8	9.89	5.10	18	.129	9	.062	93.0			--	--	------		-----	
Fluorine additive studies																						
2	186	103.3	315	2.172×10^6	9.0	4.08	49.7	22.54	5.50	158	1.089×10^6	34	0.234×10^6	101.2	421	0	--	--	------	1.9	0.574	Stable
3	142	78.9	322	2.220	8.8	3.99	53.4	24.22	6.20	177	1.220	29	.199	99.0			--	--	------		.640	Transition
5	72	40.0	202	1.393	9.9	4.49	27.1	12.29	2.73	70	.483	31	.214	99.2			--	--	------		.284	
7	101	56.1	180	1.241	6.7	3.04	24.8	11.25	3.72	44	.303	26	.179	100.4			--	--	------		.387	
10	120	66.7	341	2.351	10.6	4.81	56.3	25.5	5.30	167	1.151	22	.152	96.3			--	--	------		.551	

Extended oxidizer tube studies																				
547	70	38.9	269	1.855×10^6	11.6	5.26	45.2	20.50	3.89	81	0.558×10^6	19	0.131×10^6	93.5	100	--	--	(a)	(a)	1.9	-----	Transition
548	74	41.1	261	1.799	9.4	4.26	48.3	21.91	5.14	110	.758	21	.145	89.9	↓	--	--	(a)	(a)	↓	-----	↓
549	91	50.6	270	1.862	8.5	3.86	54.3	24.63	6.36	117	.807	22	.152	89.4		--	--	(a)	(a)		-----	
560	60	33.3	242	1.668	10.8	4.90	47.7	21.64	4.44	115	.793	20	.138	81.3		--	--	[b] $1\frac{1}{4}$	[b] 3.175			
562	61	33.9	227	1.565	8.3	3.76	54.4	24.67	6.55	155	1.069	16	.110	75.7		--	--	↓	↓		-----	
563	61	33.9	232	1.599	9.4	4.26	49.7	22.54	5.27	129	.889	14	.096	79.0		--	--				-----	
564	61	33.9	232	1.599	8.5	3.86	52.9	23.99	6.22	144	.993	13	.089	78.3	↓	--	--			↓	-----	↓
Porous injector faceplate studies																				
630	96	53.3	303	2.089×10^6	11.4	5.17	47.5	21.55	4.10	149	1.027×10^6	51	0.352×10^6	95.8	421	--	--	--	------	1.9	-----	Transition
631	114	63.3	320	2.21	9.6	4.35	54.4	24.67	5.24	113	.779	51	.352	95.4	↓	--	--	--	------	↓	-----	↓
633	118	65.6	303	2.089	8.6	3.90	55.1	24.99	5.99	111	.765	38	.262	93.8		--	--	--	------			
634	99	55.0	298	2.055	10.2	4.63	49.7	22.54	4.85	86	.593	42	.289	88.9	↓	--	--	--	------	↓	-----	↓
Nozzle area radial distribution studies																				
30	119	66.1	277	1.909×10^6	9.9	4.49	51.6	23.41	5.17	172	1.186×10^6	43	0.296×10^6	90.9	421	--	--	--	------	1.9	-----	Transition
31	90	50	289	1.993	11.8	5.35	48.3	21.91	4.09	185	1.275	42	.289	94.4	↓	--	--	--	------	↓	-----	↓
32	120	66.7	271	1.868	9.2	4.17	54.9	24.90	5.96	195	1.345	40	.276	87.7		--	--	--	------		-----	
33	111	61.7	298	2.055	11.0	4.99	51.4	23.32	4.65	196	1.351	45	.310	95.2		--	--	--	------		-----	
34	105	58.3	286	1.972	9.9	4.49	53.4	24.22	5.36	198	1.365	48	.331	91.7	↓	--	--	--	------	↓	-----	↓
Chamber wall film cooling																				
320	123	68.3	314	2.165×10^6	10.6	4.81	52.3	23.72	4.93	182	1.254×10^6	40	0.275×10^6	95.5	421	--	10	--	------	1 9	-----	Transition
321	110	61.1	317	2.186	12.6	5.71	49.5	22.45	3.94	185	1.275	43	.296	95.7		--	↓	--	------		-----	↓
322	177	98.3	308	2.124	9.6	4.35	57.0	25.86	5.93	212	1.462	54	.372	91.9		--		--	------		-----	
323	168	93.3	313	2.158	9.9	4.49	54.5	24.72	5.49	199	1.372	47	.324	95.1		--		--	------		-----	
324	120	66.7	315	2.172	11.4	5.17	50.5	22.91	4.42	165	1.138	44	.303	96.2		--	↓	--	------		-----	
331	134	74.4	311	2.144	10.5	4.76	53.1	24.10	5.04	194	1.338	0	0	93.1			20	--	------		-----	
332	114	63.3	311	2.144	12.1	5.49	48.6	22.04	3.99	173	1.193	0	0	94.9		--	↓	--	------		-----	
333	162	90	310	2.137	9.2	4.17	56.9	25.81	6.17	214	1.475	38	.262	93.1		--		--	------		-----	
335	141	78.3	307	2.117	10.8	4.89	51.0	23.13	4.71	178	1.227	52	.358	93.6		--		--	------		-----	
336	132	73.3	306	2.109	9.5	4.31	55.4	25.13	5.84	199	1.372	33	.227	92.4		--		--	------		-----	
337	141	78.3	---	---------	9.5	4.31	54.2	24.58	5.69	190	1.310	33	.227	92.1	↓	--	↓	--	------	↓	-----	↓

[a] Flush.
[b] Hastelloy.

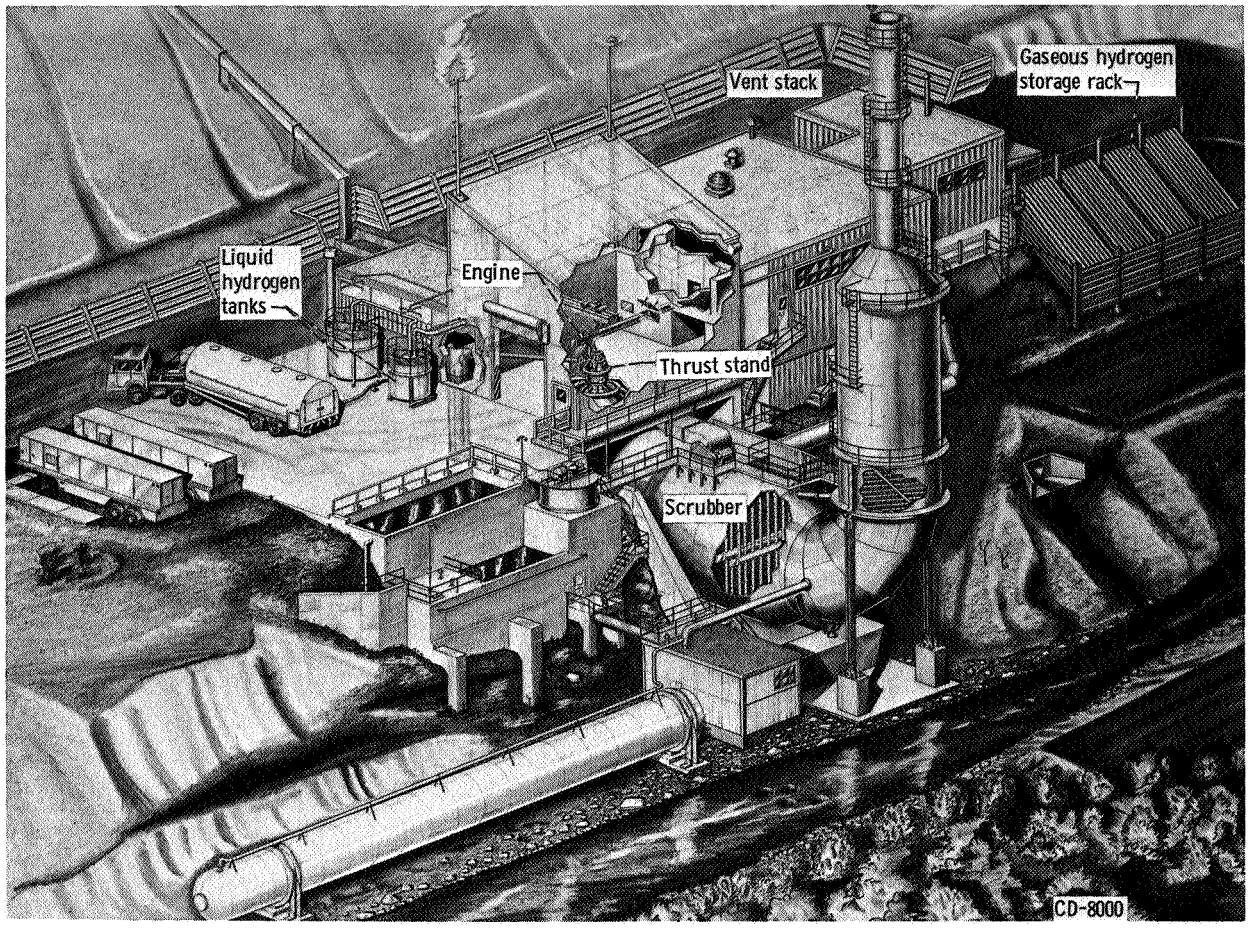

Figure 1. - Rocket engine test facility.

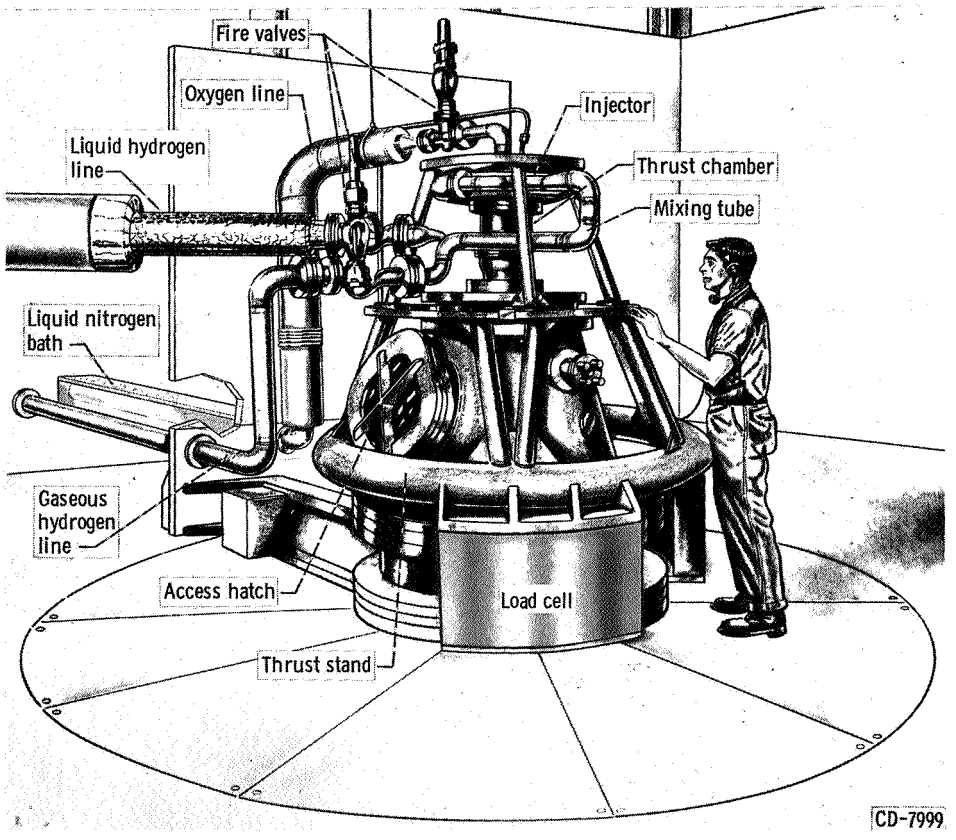

Figure 2. - Engine mounted on thrust stand..

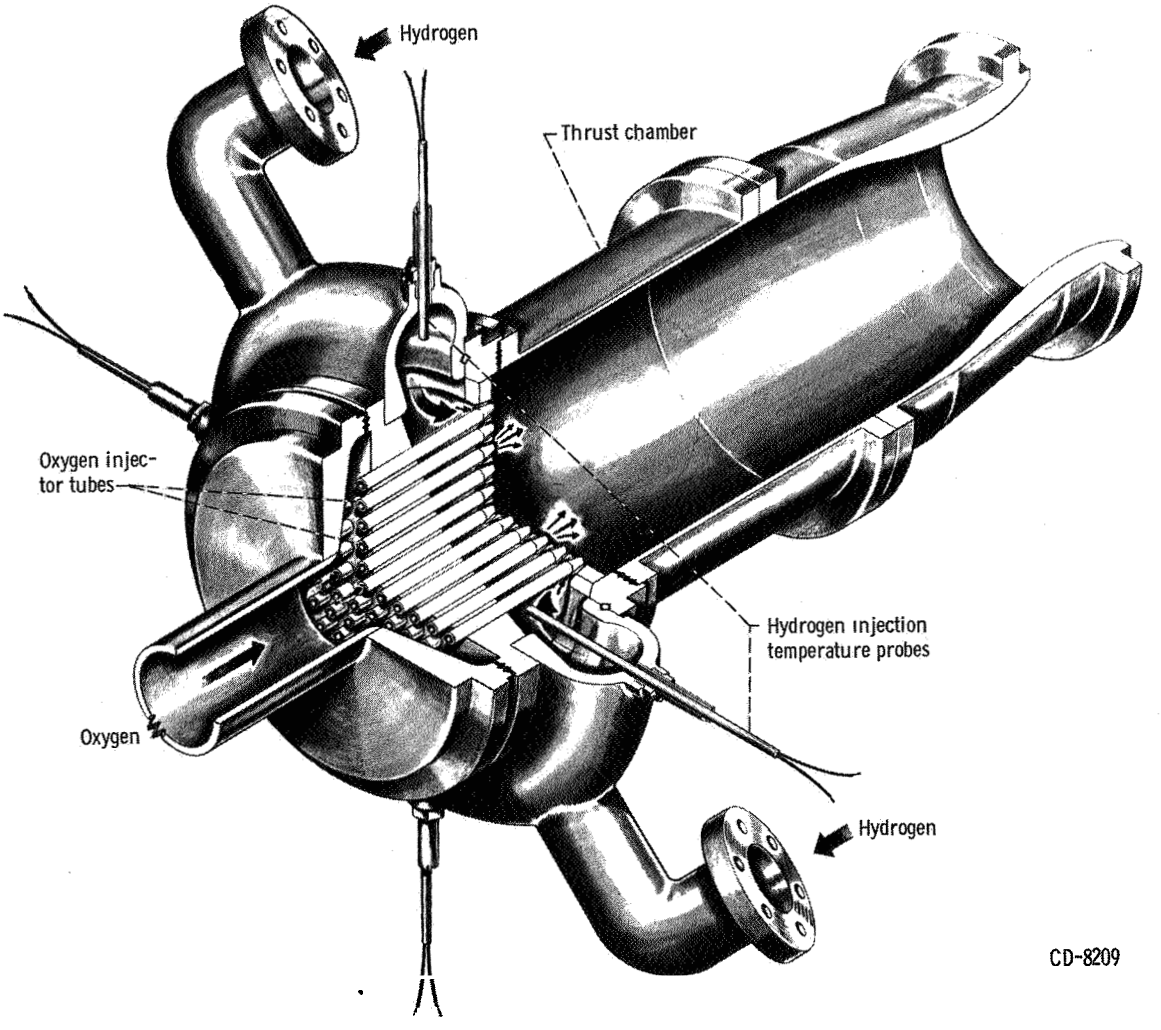

Figure 3. - Engine and injector.

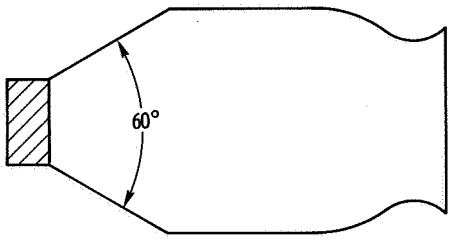

(a) 60° Tapered chamber.

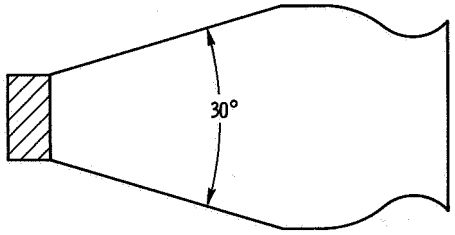

(b) 30° Tapered chamber.

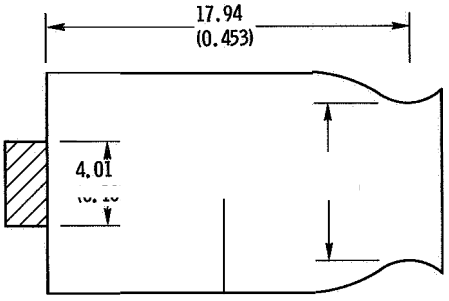

(c) Cylindrical chamber; contraction ratio A = 1.9.

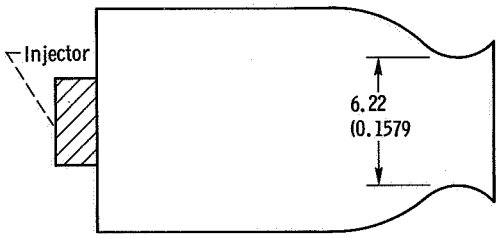

(d) Cylindrical chamber; contraction ratio A = 3.

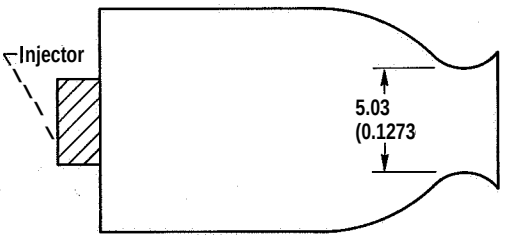

(e) Cylindrical chamber; contraction ratio A = 4.5.

Figure 4. - Thrust chamber configurations. [All dimensions in inches (and meters) unless indicated otherwise.)

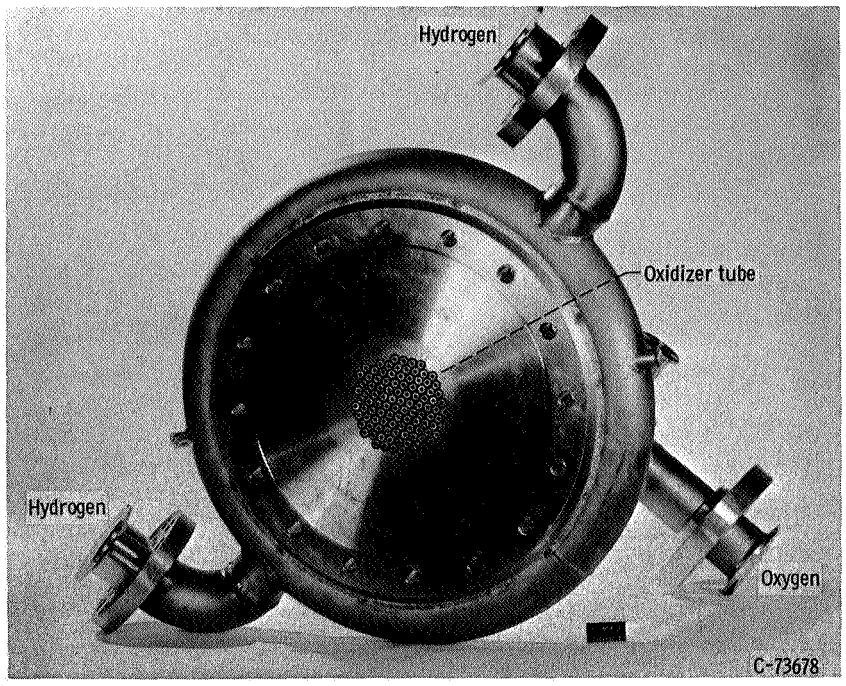

(a) Faceplate view of 100-element concentrated pattern injector.

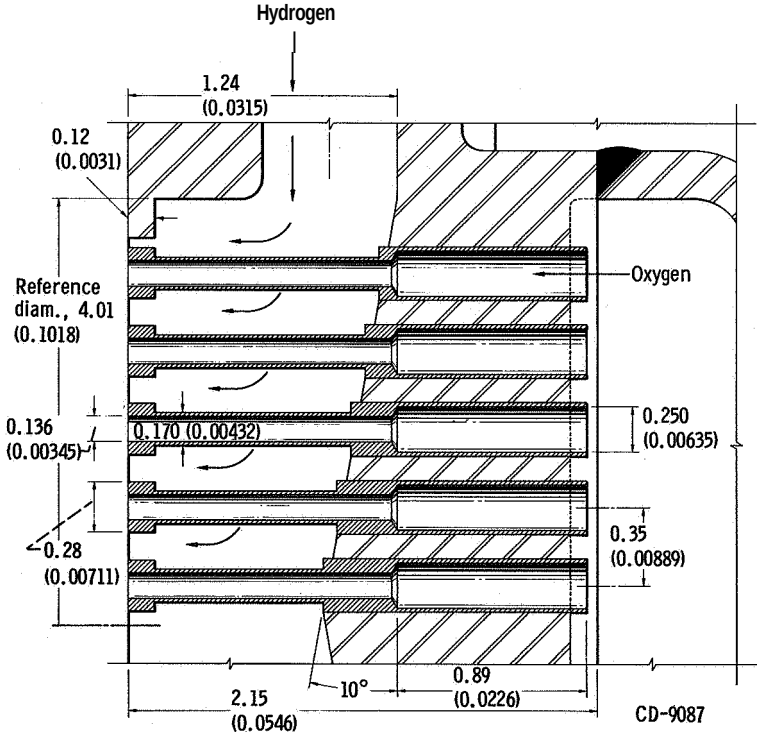

(b) Cross-sectional view of concentrated pattern injector. (All dimensions in inches land meters) unless stated otherwise.)

Figure 5. - Injector configurations.

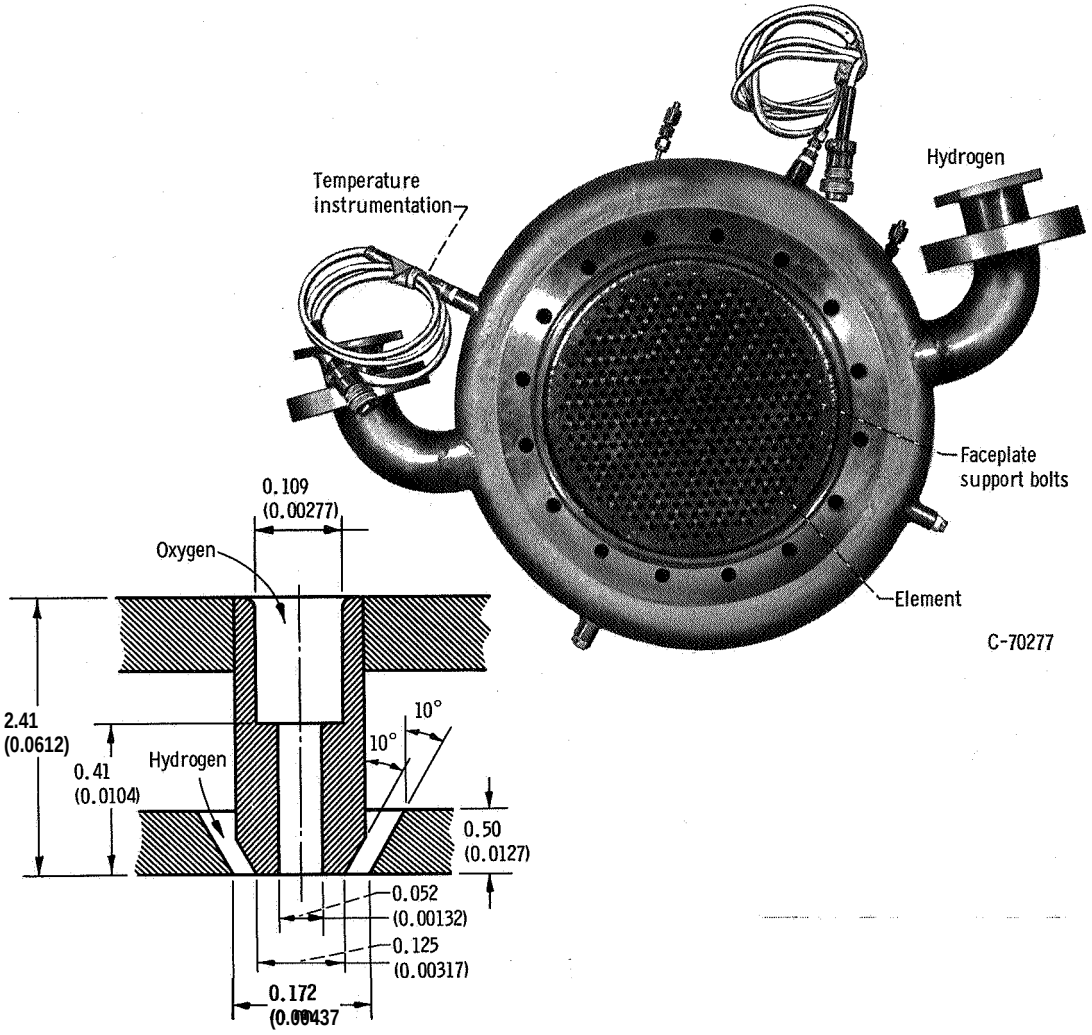

(c) Faceplate and cross-sectional views of 421-element, removable copper face, 10.78-inch-diameter (0.274-m), concentric tube injector. (All dimensions in inches (and meters) unless stated otherwise.)

Figure 5. - Continued.

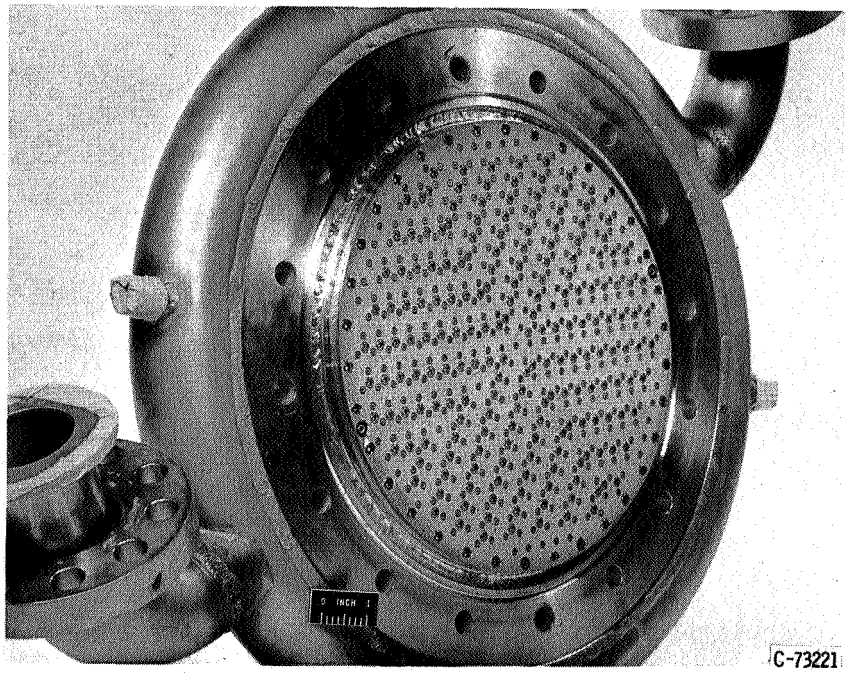

(d) Faceplate view of 421-element, porous stainless steel face concentric tube injector.

Figure 5. - Continued.

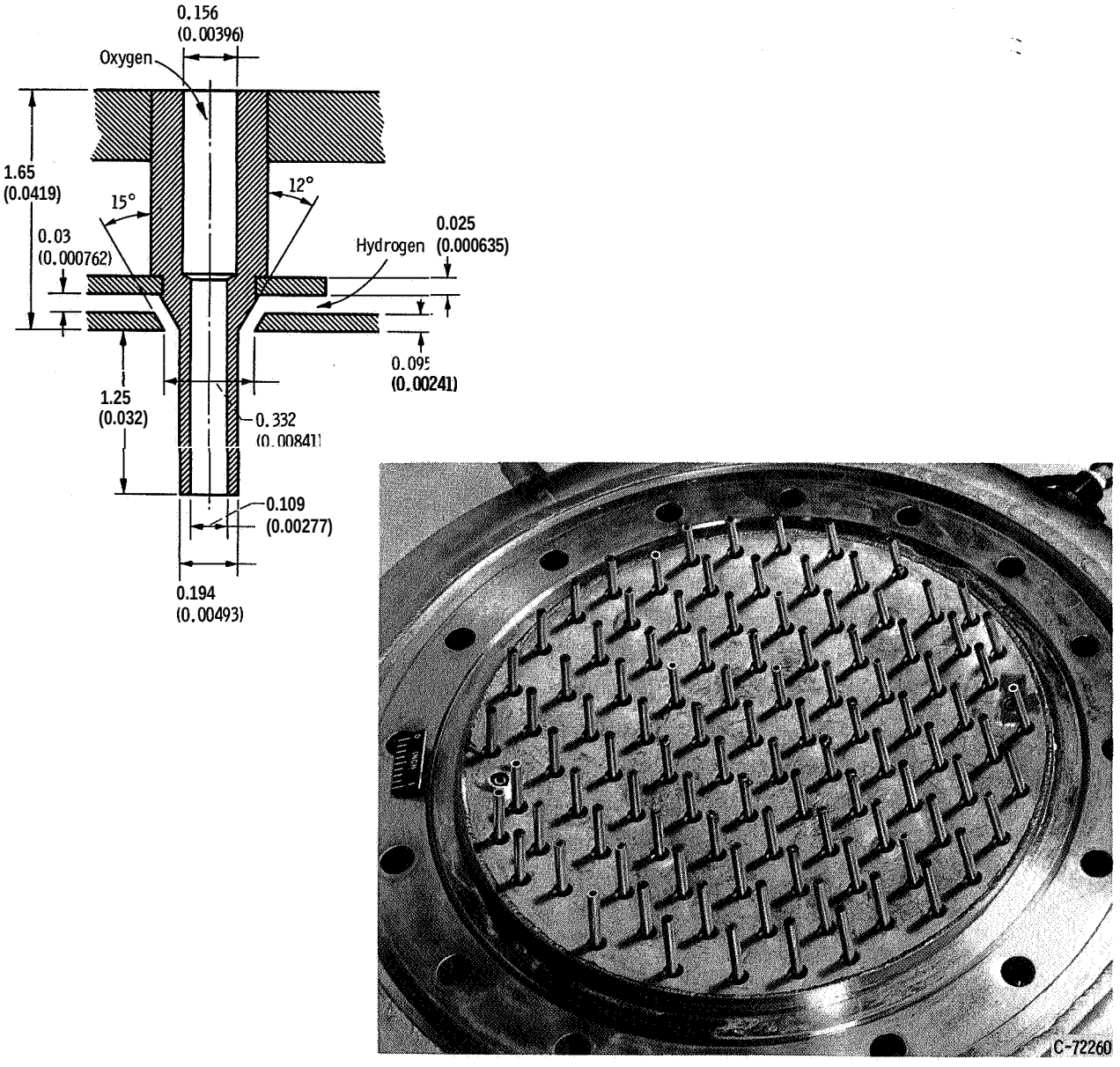

(e) Faceplate and cross-sectional views of standard 10.78-inch-diameter (0.274-m) concentric tube injector with oxidizer tubes extended 1 1/4 inches (0.032m). (All dimensions in inches (and meters) unless specified otherwise.)

Figure 5. - Concluded.

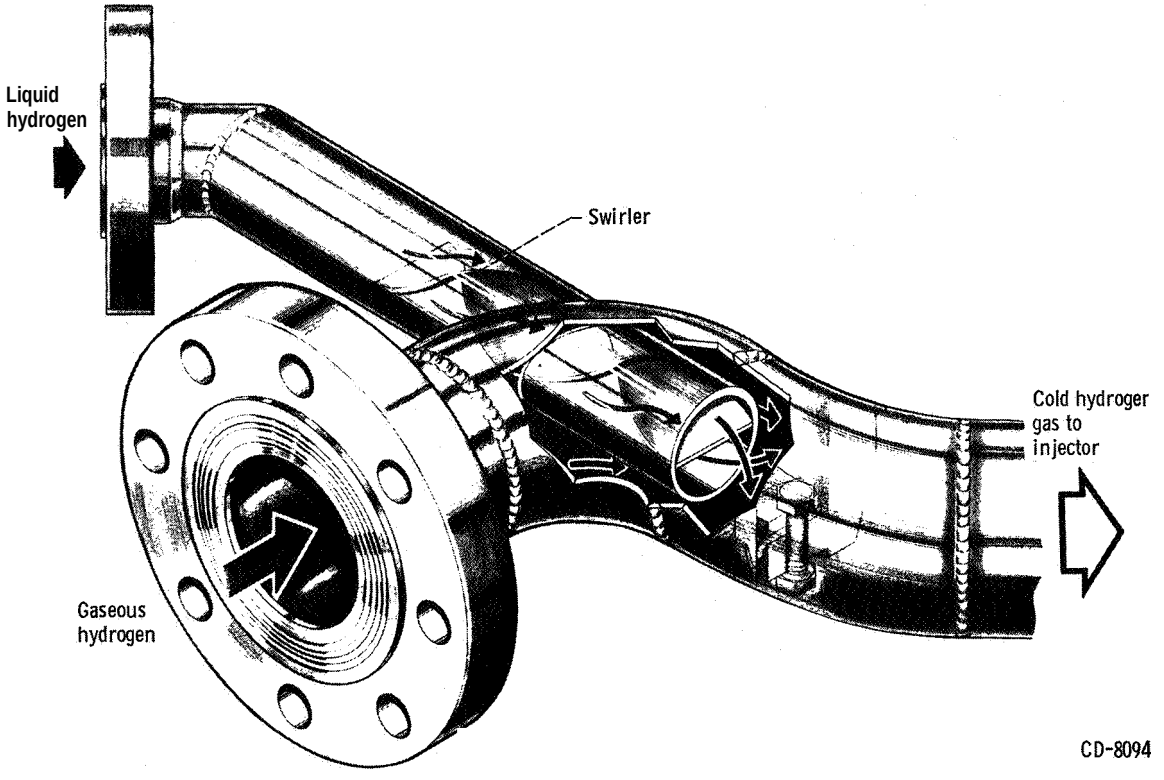

Figure 6. - Schematic of mixing station.

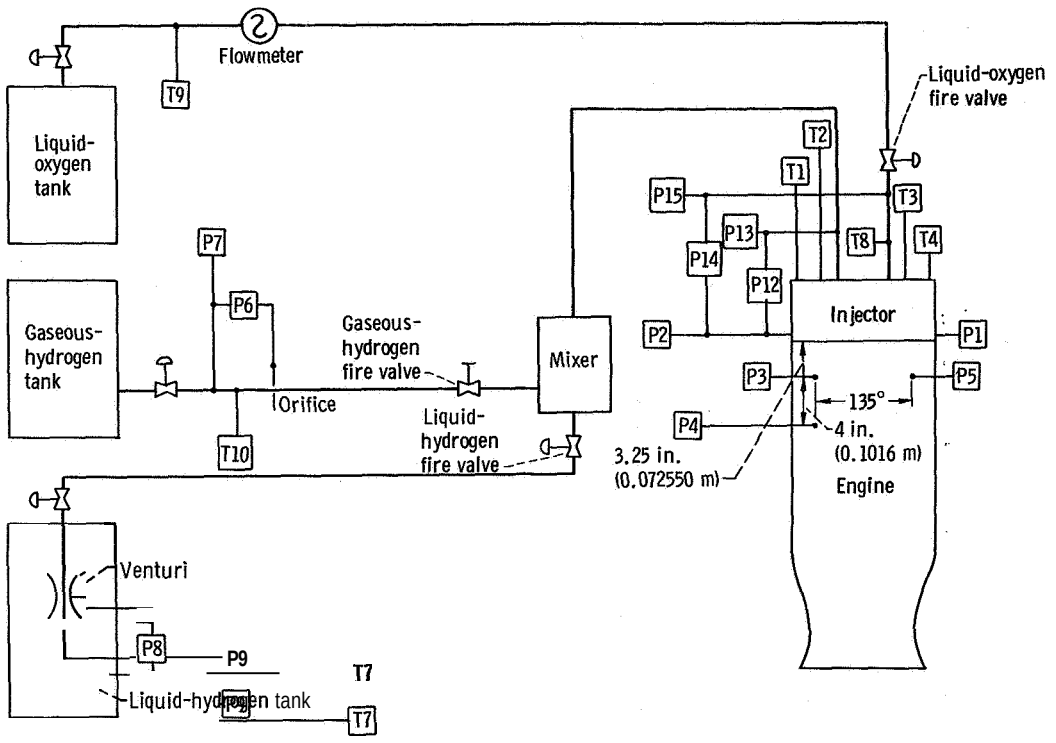

P1	Static chamber pressure (injector face), four-arm strain-gage transducer 1	P14	Oxygen-injection differential pressure, four-arm strain-gage transducer
P2	Static chamber pressure (injector face), four-arm strain-gage transducer 2	P15	Oxygen-injector pressure, four-arm strain-gage transducer
P3	Dynamic chamber pressure, water-cooled quartz pressure transducer 3	T1	Hydrogen-injector temperature, carbon-resistor-sensor probe 1
P4	Dynamic chamber pressure, water-cooled quartz pressure transducer 4	T2	Hydrogen-injectortemperature, carbon-resistor-sensor probe 2
P5	Dynamic chamber pressure, water-cooled quartz pressure transducer 5	T3	Hydrogen-injectortemperature, carbon-resistor-sensor probe 3
P6	Gaseous-hydrogenorifice differential pressure, four-ar m strain-gage transducer	T4	Hydrogen-injectortemperature, carbon-resistor-sensor probe 4
P7	Gaseous-hydrogenorifice pressure, four-arm strain-gage transducer	T7	Liquid-hydrogen venturi temperature, platinum resistor sensor
P8	Liquid-hydrogenventuri differential pressure, four-arm strain-gage transducer	T8	Oxygen-injector temperature, copper-constantan thermocouple
P9	Liquid-hydrogenventuri pressure, four-arm strain-gage transducer	T9	Oxygen flowmeter temperature, platinum resistor sensor
P12	Hydrogen-injection differential pressure, four-arm strain-gage transducer	T10	Gaseous-hydrogen orifice temperature, iron-constantan thermocouple
P13	Hydrogen-injector pressure, four-arm strain-gage transducer		

Figure 7. - Instrumentation diagram.

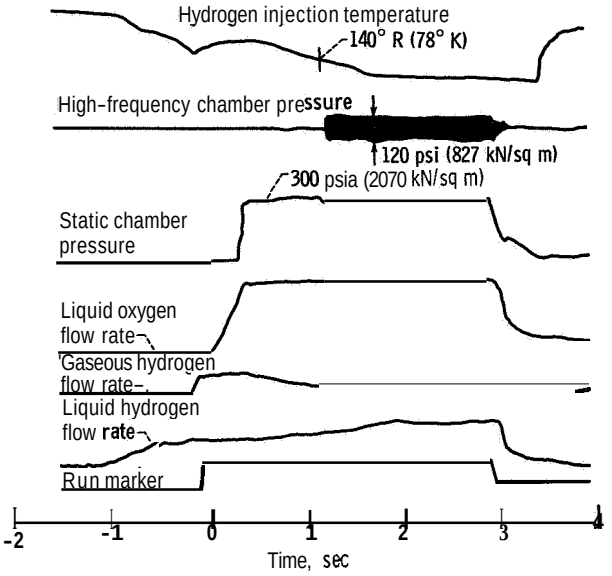

Figure 8 - Oscillograph traces of typical screech test illustrating the temperature rating technique.

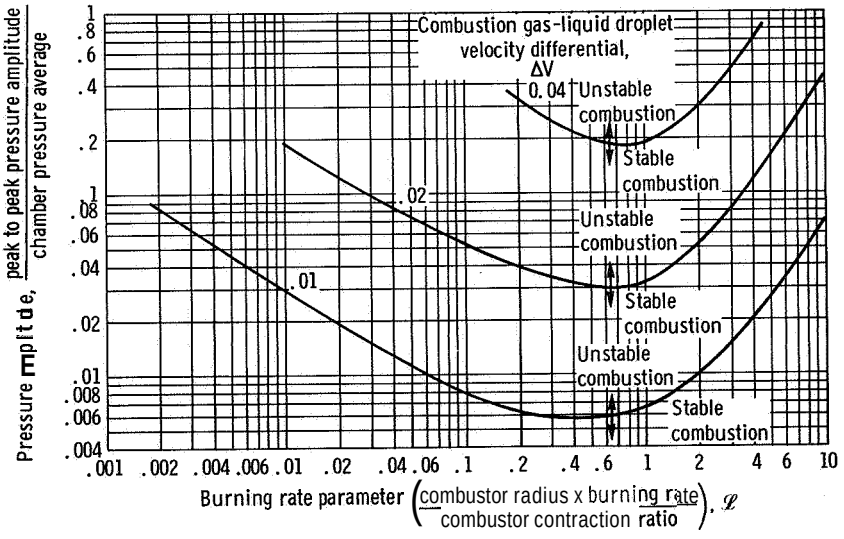

Figure 9 - Stability boundary for a vaporization rate controlled combustion process (from ref. 6).

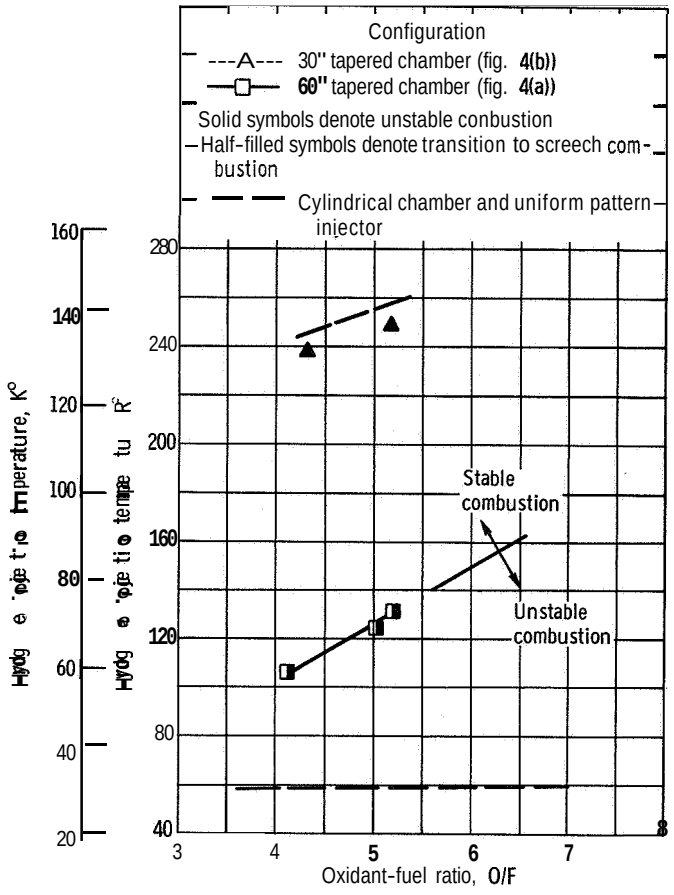

Figure 10. -Effect of injection distribution on hydrogen temperature stable operating limits of 100-element concentrated pattern injector. Contraction ratio A = 1.9.

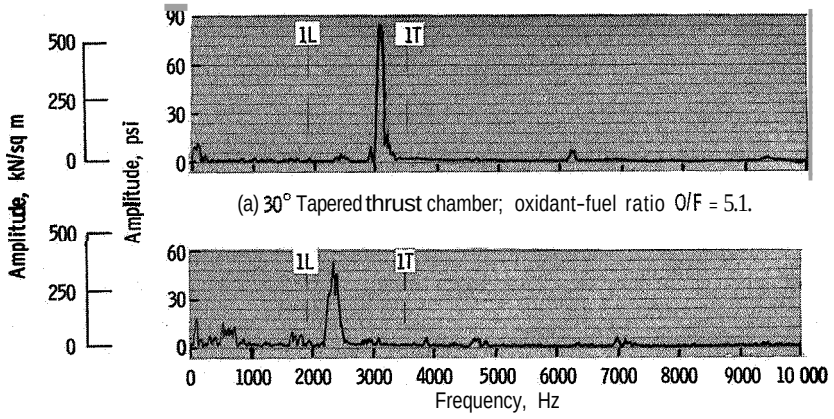

(a) 30° Tapered thrust chamber; oxidant-fuel ratio O/F = 5.1.

(b) 60° Tapered thrust chamber; oxidant-fuel ratio O/F = 5.07.

Figure 11 - Typical amplitude spectral density graphs for concentrated pattern injector with tapered thrust chambers. Amplitude, peak to peak; nozzle throat diameter, 7.82 inches (0.198628 m).

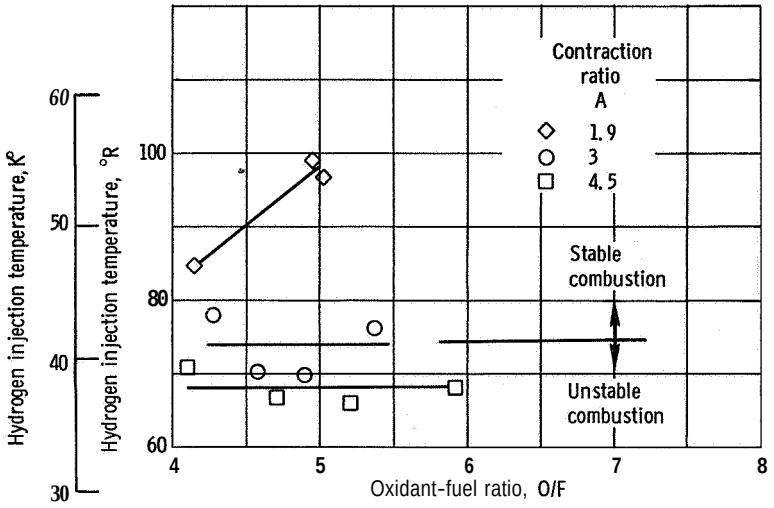

Figure 12. -Effect of contraction ratio on hydrogen temperature stable operating limits of 100-element concentrated pattern injector. Cylindrical combustion chamber of 10.78 inches (0.274 m) in diameter.

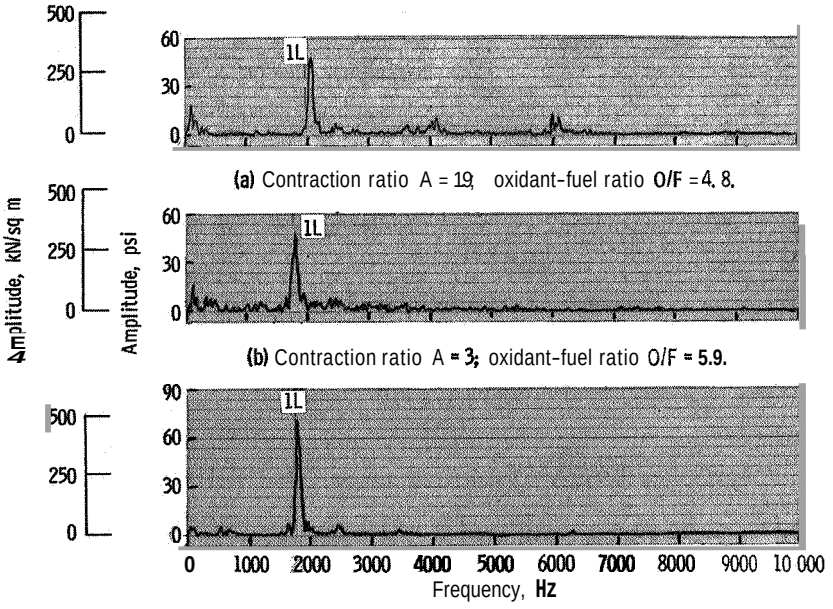

(a) Contraction ratio A = 1.9; oxidant-fuel ratio O/F = 4.8.

(b) Contraction ratio A = 3; oxidant-fuel ratio O/F = 5.9.

(c) Contraction ratio A = 4.5; oxidant-fuel ratio O/F = 5.9.

Figure 13. - Typical examples of chamber pressure oscillations during screech with concentrated pattern injector in cylindrical combustors with contraction ratios of 1.9, 3, and 4.5. Amplitude, peak to peak

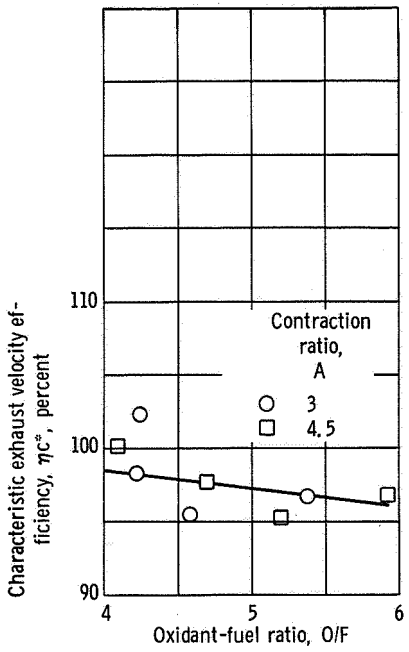

Figure 14. - Performance of 100-element concentrated pattern injector during stable operation just prior to screech. Data are for cylindrical thrust chambers.

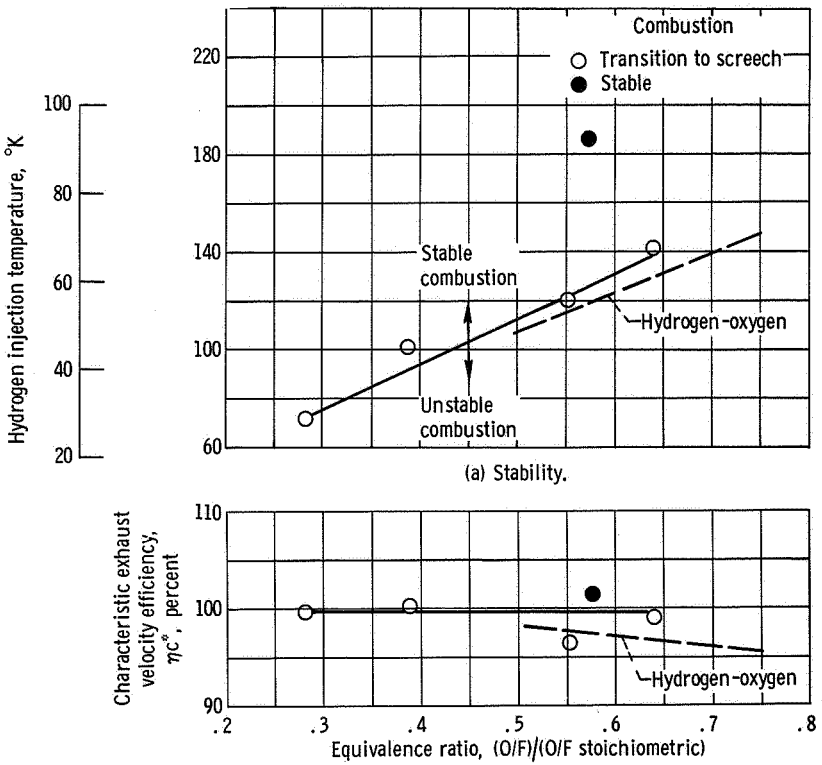

Figure 15. - Effect of fluorine additive on stability and performance of 421-element injector. Fluorine concentration, 30 percent by weight.

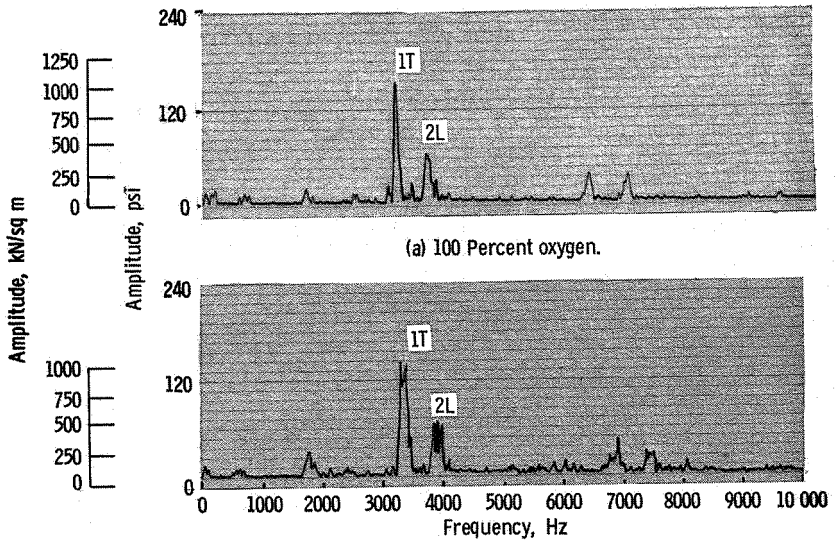

Figure 16. - Typical amplitude spectral density graphs for 421-element injector. Oxidant-fuel ratio O/F = 5.39. Amplitude, peak to peak.

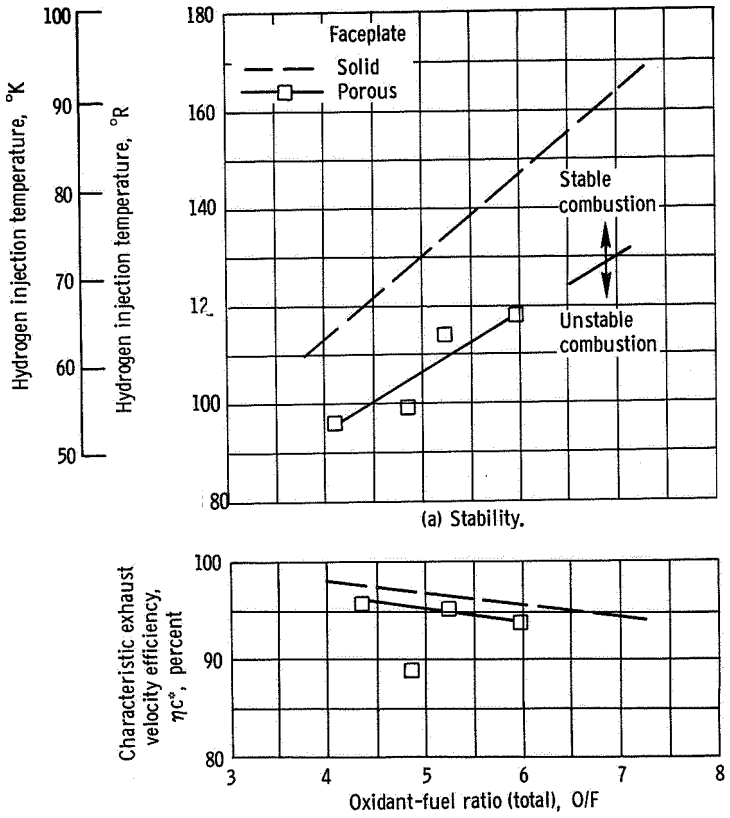

Figure 17. - Effect of porous injector faceplate on stability and performance characteristics of 421-element injector.

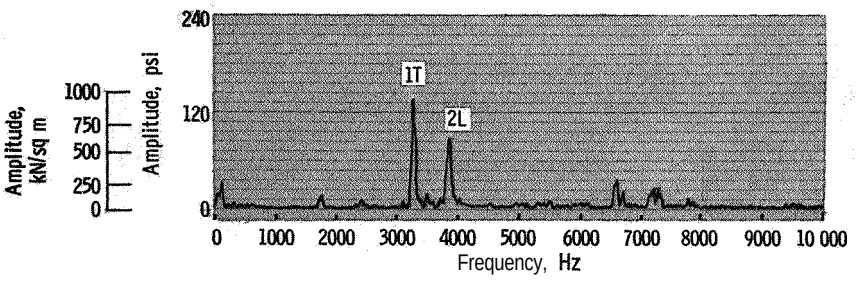

Figure 18. - Typical amplitude spectral density graph for 421-element injector with porous faceplate. Oxidant-fuel ratio O/F = 5.1. Amplitude, peak to peak

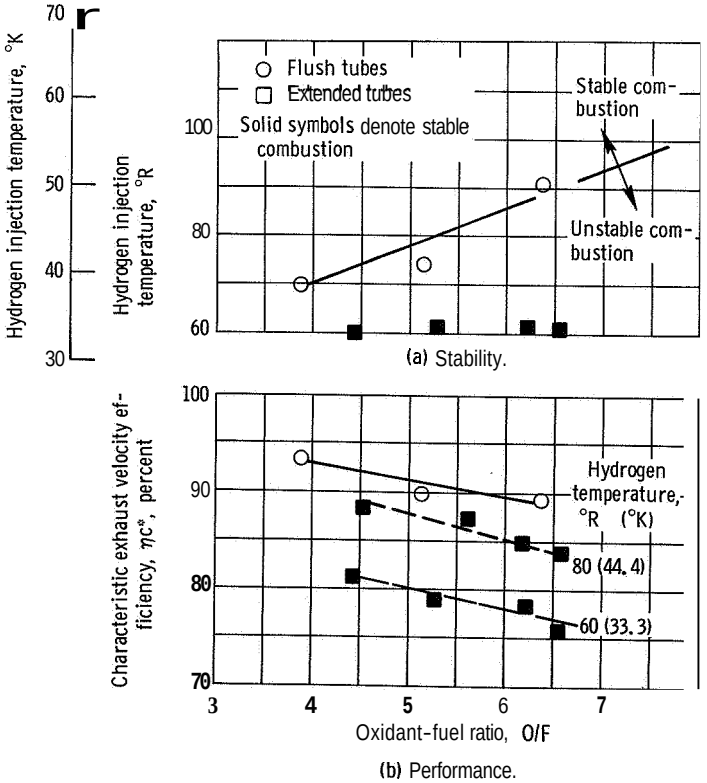

Figure 19. -Effect of oxidizer tube extension on stability and performance of 100-element injector.

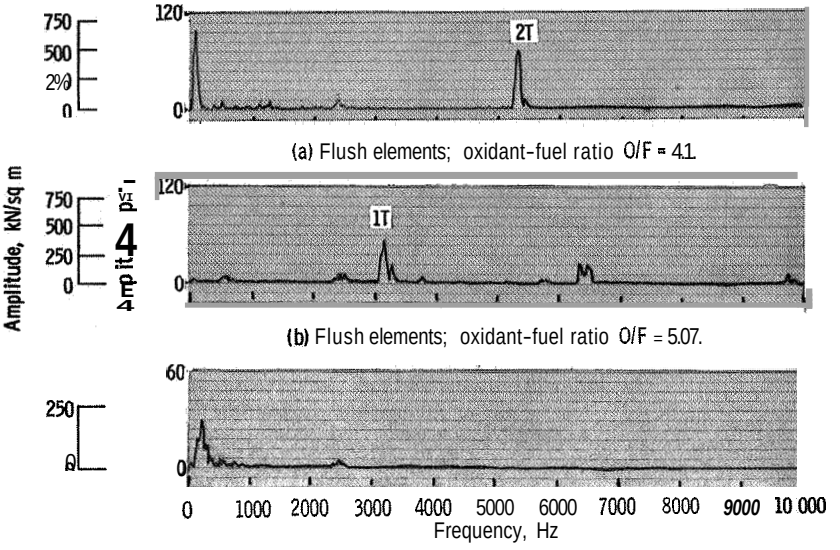

Figure 20. - Typical amplitude spectral density graphs for 100-element injector with flush and extended oxidizer tubes. Amplitude, peak to peak

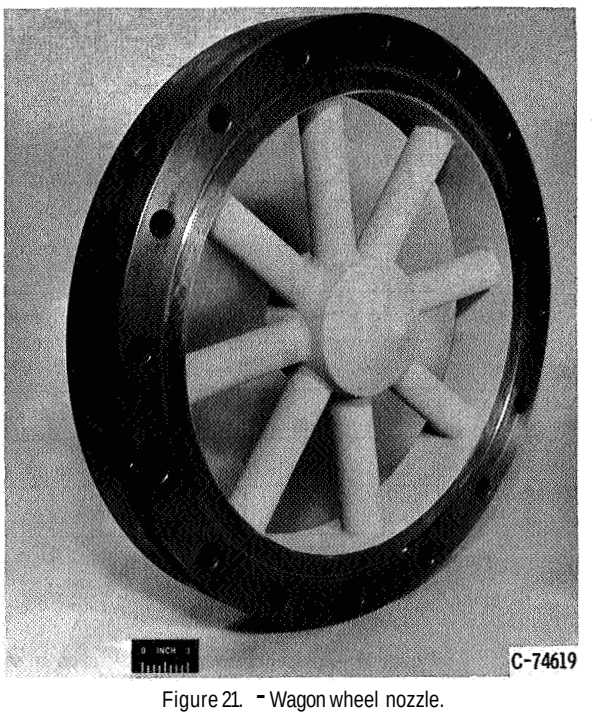

Figure 21. - Wagon wheel nozzle.

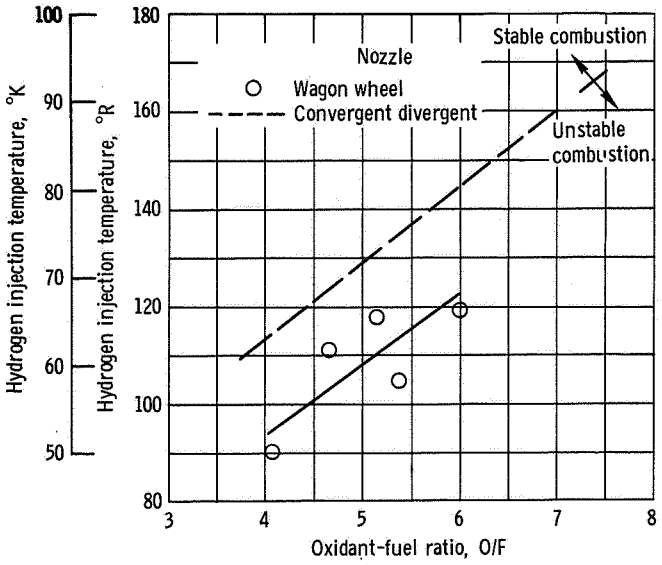

Figure 22. - Stability characteristics of combustor with convergent-divergent nozzle and with annular flow nozzle (wagon wheel).

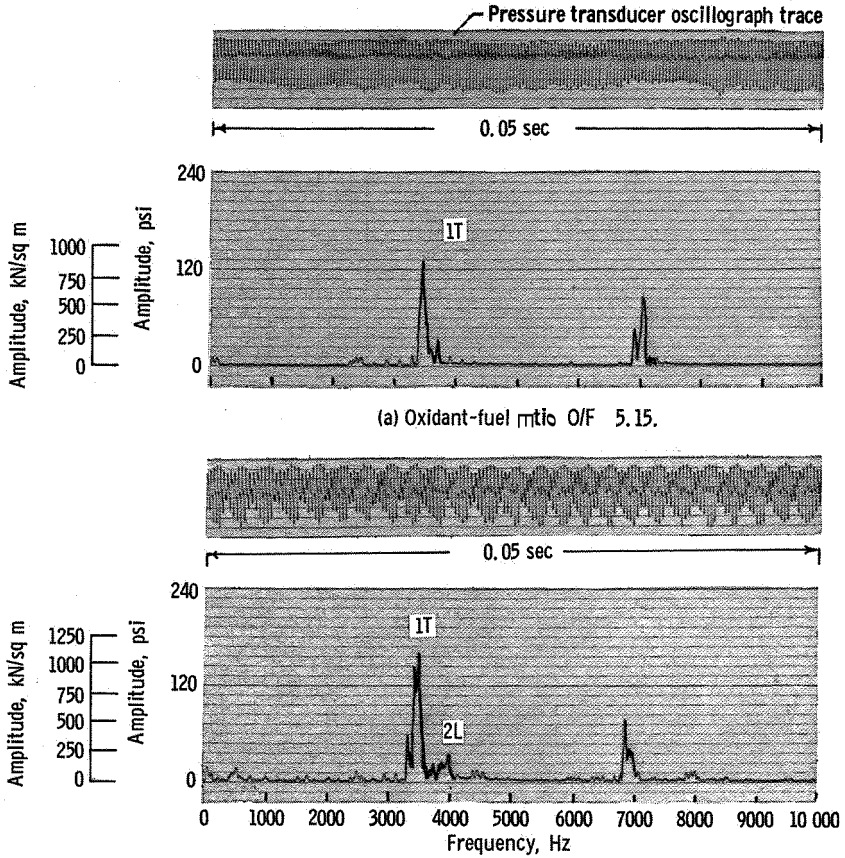

Figure 23. - Transducer oscillograph records and amplitude spectral density graphs for combustor with wagon wheel nozzle. Amplitude, peak to peak.

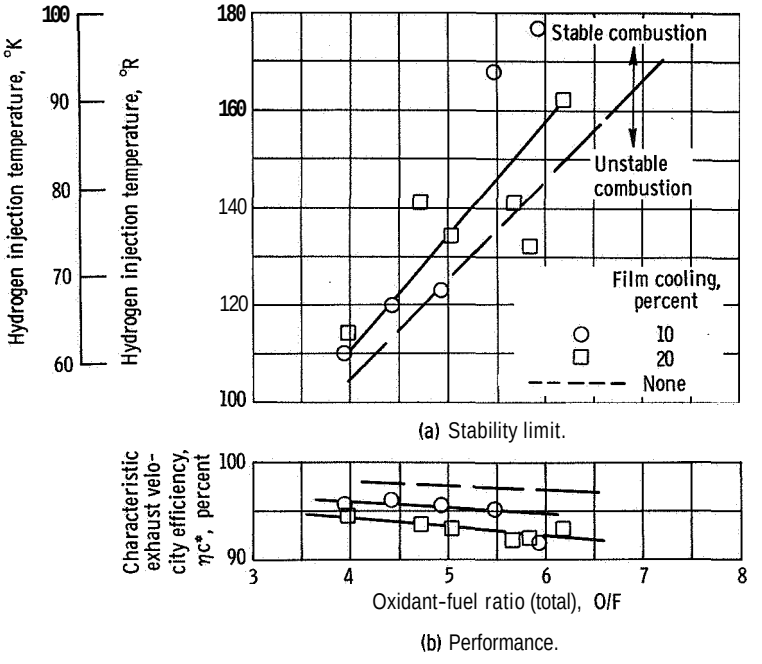

(a) Stability limit.

(b) Performance.

Figure 24. -Effect of film cooling on stability and performance of 421-element injector.